

# Quantum Algorithm for Green's Functions Measurements in the Fermi-Hubbard Model

Gino Bishop,<sup>1,2,3</sup> Dmitry Bagrets,<sup>2,4</sup> and Frank K. Wilhelm<sup>1,2</sup>

<sup>1</sup>*Theoretical Physics, Saarland University, 66123 Saarbrücken, Germany*

<sup>2</sup>*Institute for Quantum Computing Analytics (PGI-12),  
Forschungszentrum Jülich, 52425 Jülich, Germany*

<sup>3</sup>*Mercedes-Benz AG, Stuttgart, Germany*

<sup>4</sup>*Institute for Theoretical Physics, University of Cologne, 50937 Köln, Germany*

(Dated: December 7, 2023)

In the framework of the hybrid quantum-classical variational cluster approach (VCA) to strongly correlated fermion systems one of the goals of a quantum subroutine is to find single-particle correlation functions of lattice fermions in polynomial time. Previous works suggested to use variants of the Hadamard test for this purpose. However, it requires an implementation of controlled unitaries specifying the full dynamics of the simulated model. In this work, we propose a new quantum algorithm, which uses an analog of the Kubo formula within linear response theory adapted to a quantum circuit simulating the Hubbard model. It allows to access the Green's function of a cluster directly and thereby circumvents the usage of the Hadamard test. We find a drastic reduction in gate count of two-qubits gates and limitations on hardware design as compared to previous approaches.

## I. INTRODUCTION

Strongly correlated electron materials exhibit exotic phenomena such as high-temperature superconductivity [1] and Mott-insulating phases [2]. Investigating these effects and their origins is therefore crucial for promoting sophisticated material design [3], building high-fidelity superconducting qubits [4] and advanced energy storage [5]. Strong correlation arises due to Coulomb interaction between electrons and can be captured within the Fermi-Hubbard model [6].

While the Fermi-Hubbard model comprehensively incorporates electronic correlations, it is not exactly solvable beyond one dimension. Numerical methods face an inherently exponential demand in computational resources, when transitioning to larger system sizes. The landmark paper on quantum supremacy [7] has sparked great interest in the research field of quantum computation, which has now advanced to a playground for sophisticated hardware and algorithms. Strategies for solving the Fermi-Hubbard model on a quantum computer have been proposed recently [8, 9]. Among them the cluster perturbation methods [10] play a prominent role. They are capable of mitigating computational demands by dividing a lattice system into arbitrarily small, identical and disjoint clusters. The idea is to solve one of the many clusters and extrapolate the result to the full system in a self-consistent fashion. Specifically, the variational cluster approach (VCA) [11] can be used to relate the free energy of a microscopic cluster to the grand canonical potential of a macroscopic system. When the latter is found, it provides an access to the phase diagram of a given material. As the crucial step, the VCA scheme involves an evaluation of the Green's function which describes one-particle correlations in the interacting system. In practical terms it amounts to an evaluation of the Green's function using relatively small quantum

chips, which are build up of as many qubits as the number electronic orbitals contained in a cluster, plus one ancilla qubit.

A common strategy to evaluate the Green's function of a correlated system is based on the Hadamard test [12–16]. It consists of applying controlled perturbation and controlled evolution operations onto the system, implying extensive use of two-qubit gates. Here, we present a powerful alternative scheme based on linear response theory [17], which finds its application in a variety of classical scattering [18] and transport measurement experiments [19]. A linear response approach does not rely on the controlled unitary evolution and thereby shortens circuit depth. Particularly, we report an improvement in the circuit depth by reducing the number of multi-qubit gates by a factor of  $\sim 3$  which may substantially increase the performance of the VCA-based algorithms on the current NISQ devices. Also, our new scheme requires far less constrains on hardware in terms of qubit-to-qubit connectivities as compared to previous approaches.

This work is structured as follows. Section II briefly recapitulates the variational cluster approach (VCA) and may be viewed as a motivation to the efforts of investigating Green's functions. In section III we review how a unitary time evolution of the Fermi-Hubbard model can be mapped on a quantum circuit. We further introduce an algorithm based on linear response theory that is capable of outperforming the common Hadamard test in terms of circuit depth.

Section IV discusses a toy model of a two-site dimer, which we use to demonstrate the advantage of the new scheme. Lastly, Section V collects gate counts for systems with arbitrary large sizes. We conclude in Section VI, where we discuss the impact of the circuit depth reduction. We argue, that a scheme based on a direct Green's function measurement is a viable, potentially more powerful alternative to established methods such as the Hadamard test as it does not require controlled

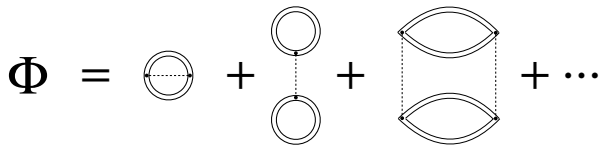


FIG. 1. The Luttinger-Ward functional  $\Phi[\mathbf{G}]$  is a sum over closed two-particle skeleton diagrams. The first summand is a particle-hole pair interacting with itself, the second summand are two particle-hole pairs interacting with each other once, the third summand are two particle-hole pairs interacting with each other twice.

unitary evolution driven by a single ancilla qubit.

## II. VARIATIONAL CLUSTER APPROACH

In this introductory section we outline the basic idea behind the variational cluster approach (VCA) [11]. The recapitulation mainly serves for the purpose of demonstrating the usefulness of the quantum algorithms aimed at finding the correlation functions of moderately large clusters and their potential speed-up over purely classical methods of computation. We also introduce the Hamiltonian of the Hubbard model and the notation to be used across the paper.

The VCA is a method that allows for solving many-body systems in a self-consistent manner. In general, we assume that a many-body system is described by a lattice Hamiltonian  $H$  of macroscopic size. While the number of qubits needed to encode the full Hilbert space of  $H$  scales exponentially with the number of sites, the VCA enables one to reduce the number of required qubits by investigating only a small, representative subset, i.e. a cluster, of the full lattice. These clusters are disjoint, identical copies of each other, whose Hamiltonian is denoted as  $H'$ . Since the cluster acts as a proxy to the full system, meaningful investigations can be carried out with a relatively small quantum chip.

The Fermi-Hubbard model [20], which is widely used to describe the physics of strongly correlated electrons, is a prototypical example where VCA can be successfully applied.

The Fermi-Hubbard model is described via a Hamiltonian of the form  $H = H_0(\mathbf{t}) + H_1(\mathbf{U})$ . It is a sum of a kinetic short-range hopping term characterized by amplitudes  $\mathbf{t}$  and a repulsive on-site interaction of strength  $\mathbf{U}$ :

$$\hat{H} = \sum_{\langle i,j \rangle, \sigma} t_{ij} \hat{c}_{i,\sigma}^\dagger \hat{c}_{j,\sigma} + \sum_i U_i \hat{n}_{i,\uparrow} \hat{n}_{i,\downarrow}. \quad (1)$$

Here, the operators  $c_{i,\sigma}$  and  $c_{i,\sigma}^\dagger$  destroy or create an electron with spin  $\sigma$  on the  $i$ -th site, respectively,  $\hat{n}_{i,\sigma} = c_{i,\sigma}^\dagger c_{i,\sigma}$  are number operators, and the summation in the kinetic term goes over nearest neighbours.

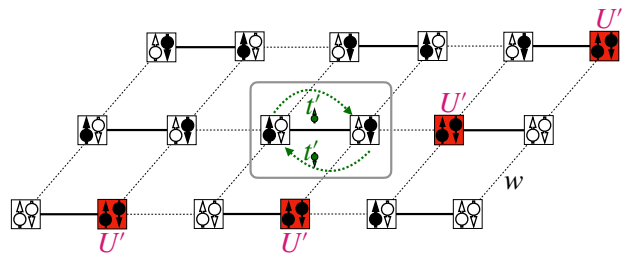


FIG. 2. (Color online) 2D lattice representing the Fermi-Hubbard model at half-filling. Each site can be occupied by at most two fermions. Dashed lines show the allowed hopping to neighboring sites. Two fermions occupying a single site experience a Coulomb repulsion  $U$ .

A microscopically small cluster described by  $H'$  can not lead to long-range effects such as magnetism and superconductivity, which arise in the macroscopic system described by the full  $H$ . In order to impose these effects in the cluster, we can add symmetry breaking terms to the Hamiltonian which may promote different superconducting, ferromagnetic or charge-density orders. A connection between micro- and macroscopic systems is established via their grand potentials. In particular, following Luttinger and Ward [21], one can consider the grand canonical potential of interacting fermions to be a functional of the Green's function  $\mathbf{G}$  and the self-energy  $\mathbf{\Sigma}$ ,

$$\Omega_{\mathbf{t}}[\mathbf{G}, \mathbf{\Sigma}] = -\text{Tr} \ln(\mathbf{G}_0^{-1} - \mathbf{\Sigma}) - \text{Tr}(\mathbf{G}\mathbf{\Sigma}) + \Phi[\mathbf{G}], \quad (2)$$

where  $\mathbf{G}_0^{-1}$  is the non-interacting Green's function and  $\Phi[\mathbf{G}]$  is the Luttinger-Ward functional. Diagrammatically, the latter can be defined as a sum over all irreducible two-particle diagrams, referred to as skeleton diagrams, Fig. 1. In the expression above both the Green's function,  $G_{\tau_1 \tau_2}^{\alpha \beta}$ , and the self-energy,  $\Sigma_{\tau_1 \tau_2}^{\alpha \beta}$ , have to be understood as matrices in position, spin and (Matsubara) time domains, with Greek letters,  $\alpha = (i, \sigma)$ , being used as combined indices in lattice and spin spaces. The functional  $\Omega_{\mathbf{t}}[\mathbf{G}, \mathbf{\Sigma}]$  achieves its stationary value at the physical  $\mathbf{G}$  and  $\mathbf{\Sigma}$ . In particular, a functional derivative of the Luttinger-Ward functional gives the diagrammatic expansion for the self-energy,

$$\delta \Phi[\mathbf{G}] / \delta \mathbf{G} = \mathbf{\Sigma}[\mathbf{G}]. \quad (3)$$

This relation guarantees that  $\delta \Omega_{\mathbf{t}}[\mathbf{G}, \mathbf{\Sigma}] / \delta \mathbf{G} = 0$ . On the other hand, optimization over the self-energy yields the exact Dyson equation,

$$\frac{\delta \Omega_{\mathbf{t}}[\mathbf{G}, \mathbf{\Sigma}]}{\delta \mathbf{\Sigma}} = 0 \Rightarrow (\mathbf{G}_0^{-1} - \mathbf{\Sigma})\mathbf{G} = \mathbf{1}. \quad (4)$$

The variational principle outlined above can be simplified if one assumes that one can resolve (3) by defining the Green's function  $\mathbf{G} = \mathbf{G}[\mathbf{\Sigma}]$  in terms of the self-energy. The functional (2) then reduces to

$$\Omega_{\mathbf{t}}[\mathbf{\Sigma}] = -\text{Tr} \ln(\mathbf{G}_0^{-1} - \mathbf{\Sigma}) + F[\mathbf{\Sigma}], \quad (5)$$

where we have introduced the Legendre transform of the Luttinger-Ward functional,

$$F[\Sigma] = \Phi[\mathbf{G}[\Sigma]] - \text{Tr}(\Sigma\mathbf{G}[\Sigma]), \quad (6)$$

which satisfies  $\delta F[\Sigma]/\delta\Sigma = \mathbf{G}[\Sigma]$ . It follows that  $\Omega_{\mathbf{t}}[\Sigma]$  is stationary at the physical self-energy, since the condition  $\delta\Omega_{\mathbf{t}}[\Sigma]/\delta\Sigma = 0$  constitutes the Dyson equation (4).

The Luttinger-Ward functional, and hence  $F[\Sigma]$ , is not known in general [22], cf. [23]. However it is universal in the sense that it is defined only by the interaction part of the Hamiltonian,  $H_1(\mathbf{U})$ , and is independent of  $H_0(\mathbf{t})$ . This observation has motivated Potthoff to restrict the class of variational self-energies to those which optimize the functional  $\Omega_{\mathbf{t}}[\Sigma]$  for the reference system of disjoint clusters described by the Hamiltonian  $H = H_0(\mathbf{t}') + H_1(\mathbf{U})$ . Denoting the (exact) solution of this optimization problem by  $\Sigma_{\mathbf{t}'}$ , one can relate the original functional  $\Omega_{\mathbf{t}}[\Sigma]$  of the physical system to the reference one,  $\Omega_{\mathbf{t}} \equiv \Omega_{\mathbf{t}'}[\Sigma_{\mathbf{t}'}]$ , by a simple relation

$$\Omega_{\mathbf{t}}[\Sigma_{\mathbf{t}'}] = \Omega_{\mathbf{t}'} - \text{Tr} \ln(\mathbf{G}_0^{-1} - \Sigma_{\mathbf{t}'}) + \text{Tr} \ln(\mathbf{G}'_0^{-1} - \Sigma_{\mathbf{t}'}),$$

where  $\mathbf{G}'_0$  represents the free fermion propagator of a cluster. The above approximate functional can be rewritten in the Fourier space with the help of Matsubara sums and treating a single cluster as a unit cell of the infinite size physical system,

$$\Omega_{\mathbf{t}}[\Sigma_{\mathbf{t}'}] = \Omega_{\mathbf{t}'} - T \sum_{\omega_n, \mathbf{k}} \text{Tr} \ln(1 - V_{\mathbf{k}}\mathbf{G}'(\omega_n)), \quad (7)$$

where  $\mathbf{G}'(\omega_n) = (i\omega_n - \mathbf{t}' - \Sigma_{\mathbf{t}'}(\omega_n))^{-1}$  is the cluster Green's function expressed through the corresponding self-energy with  $V_{\mathbf{k}} = \mathbf{t}' - \mathbf{t}_{\mathbf{k}}$  being a matrix of inter-cluster hopping terms.

The self-consistency scheme of the VCA then substitutes the variational principle in Eq. (4) by optimizing (7) over inter-cluster parameters  $\mathbf{t}'$ . The latter may include different mean-field order parameters related to expected patterns of symmetry breaking, which are not a part of the microscopic Hamiltonian (1). Such optimization procedure over  $\mathbf{t}'$  requires an efficient evaluation of the Green's function  $\mathbf{G}$ , which turns out to be the computationally most demanding task and is thereby delegated to quantum hardware. Indeed, let  $N_c$  be the number of sites per cluster. On taking into account spin, the dimension of its Hilbert space grows exponentially as  $D = 4^{N_c}$ , thus brute-force classical computations need to operate with  $D \times D$  linear problems. On other hand, an alternative computation of a cluster Green's function  $\mathbf{G}'$  using a quantum circuit requires measurements of only  $\mathcal{O}(N_c^2)$  site-to-site correlation functions, while the number of qubits scales as  $N_c$ . Based on this idea, we show in the remainder of this paper a new efficient route how to evaluate the Green's function on a quantum computer.

Gate	Symbol	Matrix
Hadamard		$\frac{1}{\sqrt{2}} \begin{pmatrix} 1 & 1 \\ 1 & -1 \end{pmatrix}$
X		$\begin{pmatrix} 0 & 1 \\ 1 & 0 \end{pmatrix}$
Z		$\begin{pmatrix} 1 & 0 \\ 0 & -1 \end{pmatrix}$
Z-rotation		$\begin{pmatrix} e^{-i\theta/2} & 0 \\ 0 & e^{i\theta/2} \end{pmatrix}$
Y-basis change		$\frac{1}{\sqrt{2}} \begin{pmatrix} 1 & -i \\ -i & 1 \end{pmatrix}$
Phase		$\begin{pmatrix} 1 & 0 \\ 0 & e^{i\theta} \end{pmatrix}$
Controlled-Not		$\begin{pmatrix} 1 & 0 & 0 & 0 \\ 0 & 1 & 0 & 0 \\ 0 & 0 & 0 & 1 \\ 0 & 0 & 1 & 0 \end{pmatrix}$
Controlled-Z		$\begin{pmatrix} 1 & 0 & 0 & 0 \\ 0 & 1 & 0 & 0 \\ 0 & 0 & 1 & 0 \\ 0 & 0 & 0 & -1 \end{pmatrix}$

TABLE I. Full list of applied gates in matrix representation.

### III. CIRCUIT REPRESENTATION OF THE HUBBARD MODEL

We start this section by reviewing well known results in the literature [9] on how a unitary time evolution of the Fermi-Hubbard model can be represented by a quantum circuit and further on introduce an algorithm for the Green's function measurement based on the linear response theory.

#### A. Quantum circuits for hopping and repulsion terms

To construct an evolution operator of the cluster Hubbard Hamiltonian related to a single Trotter step, one needs to map fermionic operators to the qubit ones. This can be achieved in two stages. First, we introduce *Majorana fermions*,  $x_{i\sigma} = c_{i\sigma} + c_{i\sigma}^\dagger$  and  $y_{i\sigma} = i(c_{i\sigma} - c_{i\sigma}^\dagger)$ , which are Hermitian operators. They obey to the anti-commutation relations

$$\begin{aligned} \{x_{i\sigma}, x_{j\sigma'}\} &= \{y_{i\sigma}, y_{j\sigma'}\} = 2\delta_{ij}\delta_{\sigma\sigma'}, \\ \{x_{i\sigma}, y_{j\sigma'}\} &= 0. \end{aligned} \quad (8)$$

At the second stage, the Jordan-Wigner transformation is used to represent  $x_{i\sigma}$  and  $y_{i\sigma}$  via the following sequences

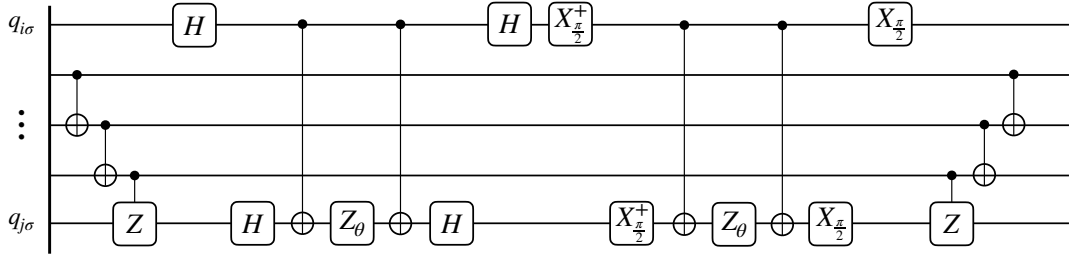


FIG. 3. Hopping circuit to evaluate the term  $t_{ij}(c_{i,\sigma}^\dagger c_{j,\sigma} + \text{h.c.})$  for a time step  $\Delta\tau$  with angle  $\theta = t_{ij}\Delta\tau$ .

of  $X$ -,  $Y$  and  $Z$ -gates:

$$\begin{aligned} x_{i\uparrow} &= \mathbb{1}^{\otimes 2(N_c-i)+1} \otimes X \otimes Z^{\otimes 2(i-1)}, \\ x_{i\downarrow} &= \mathbb{1}^{\otimes 2(N_c-i)} \otimes X \otimes Z^{\otimes 2i-1}, \\ y_{i\uparrow} &= -\mathbb{1}^{\otimes 2(N_c-i)+1} \otimes Y \otimes Z^{\otimes 2(i-1)}, \\ y_{i\downarrow} &= -\mathbb{1}^{\otimes 2(N_c-i)} \otimes Y \otimes Z^{\otimes 2i-1}, \end{aligned} \quad (9)$$

which guarantees satisfiability of the anti-commutation relations (8). Consequently, we define the correlation function for original fermions,

$$iG_{ij}^{\sigma\sigma'}(\tau) = \begin{pmatrix} \langle c_{i\sigma}(\tau) c_{j\sigma'}^\dagger(0) \rangle & \langle c_{i\sigma}(\tau) c_{j\sigma'}(0) \rangle \\ \langle c_{i\sigma}^\dagger(\tau) c_{j\sigma'}^\dagger(0) \rangle & \langle c_{i\sigma}^\dagger(\tau) c_{j\sigma'}(0) \rangle \end{pmatrix}, \quad (10)$$

and for Majorana ones

$$ig_{ij}^{\sigma\sigma'}(\tau) = \begin{pmatrix} \langle x_{i\sigma}(\tau) x_{j\sigma'}(0) \rangle & \langle x_{i\sigma}(\tau) y_{j\sigma'}(0) \rangle \\ \langle y_{i\sigma}(\tau) x_{j\sigma'}(0) \rangle & \langle y_{i\sigma}(\tau) y_{j\sigma'}(0) \rangle \end{pmatrix}, \quad (11)$$

then the two are related by a unitary transformation

$$G_{ij}^{\sigma\sigma'}(\tau) = \frac{1}{2} M^\dagger g_{ij}^{\sigma\sigma'}(\tau) M, \quad M = \frac{1}{\sqrt{2}} \begin{pmatrix} 1 & 1 \\ i & -i \end{pmatrix}. \quad (12)$$

For the sake of generality, we do not imply any time ordering in the definition of the Green's functions.

Following [9], we then present quantum circuits for a time step  $\Delta\tau$  for both hopping and repulsion as per the Fermi-Hubbard model, Eq. (1). A circuit for the hopping term is shown in Fig. 3 and a circuit for the repulsion can be seen in Fig. 4. Here, the gate  $X_{\pi/2}$  here refers to the  $Y$ -basis change gate. A complete list of applied gates in matrix representation is presented in Table I.

For our subsequent discussion of the Green's function measurement scheme (see Sec. III D 2) it is instructive to

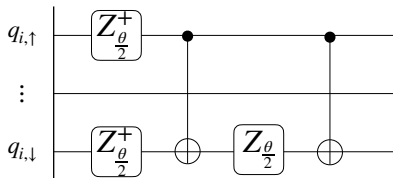


FIG. 4. Repulsion circuit to evaluate the term  $U_i n_{i,\uparrow} n_{i,\downarrow}$  for a time step  $\Delta\tau$  with angle  $\theta = U_i\Delta\tau$ .

rationalize the circuit behind the hopping term, shown in Fig. 3. To this end we note that its representation in terms of Majorana fermions reads

$$h_{ij}^{\sigma\sigma} = c_{i\sigma}^\dagger c_{j\sigma} + \text{h.c.} = \frac{i}{2} (y_{i\sigma} x_{j\sigma} - x_{i\sigma} y_{j\sigma}). \quad (13)$$

The Jordan-Wigner transformation (9) reduces the above operator to

$$h_{ij}^{\sigma\sigma} = \frac{1}{2} (X_m X_n + Y_m Y_n) Z_{\text{JW}}(m, n), \quad (14)$$

where  $m = 2i + (1 - \sigma)/2$ ,  $n = 2j + (1 - \sigma)/2$  and  $Z_{\text{JW}}(m, n)$  stands for the Jordan-Wigner string,

$$Z_{\text{JW}}(m, n) = \bigotimes_{k=m+1}^{n-1} Z_k, \quad (15)$$

with Pauli operators  $X_k$ ,  $Y_k$  and  $Z_k$  acting on  $k$ -th qubit. We can then introduce unitary Clifford gates  $S_{mn}$  acting on all qubits  $k$  with  $m < k < n$  (its equivalent circuit is shown in Fig. 6), for which the role is to eliminate the Jordan-Wigner string and simplify (14) to

$$h_{ij}^{\sigma\sigma} = \frac{1}{2} S_{mn}^\dagger (X_m X_n + Y_m Y_n) S_{mn}. \quad (16)$$

The  $XX$ - and  $YY$ -terms above commute, so that an evolution operator generated by  $h_{ij}^{\sigma\sigma}$  naturally splits into the product of two. Subsequent unitary transformations using single qubit gates  $H$  and  $X_{\pi/2}$  transform each term of the sum in Eq. (16) to the product  $Z_m \otimes Z_n$ . After that, the unitary evolution corresponding to a single Trotter step of a hopping operator with an angle  $\theta = t_{ij}\Delta\tau$  is realized with the help of  $Z$ -rotations and additional similarity transformations with CNOT gates, as shown in Fig. 3.

## B. Variational Hamiltonian ansatz (VHA) for the ground state

The correlation functions defined by Eq. (10) presume the average over the equilibrium density matrix. At zero temperature one is required to start from the ground state of the cluster at time  $\tau = 0$ . For this reason we will

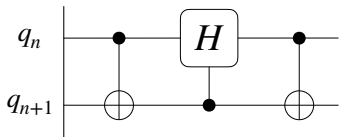


FIG. 5. Circuit for diagonalizing  $\frac{1}{2}(X_n X_{n+1} + Y_n Y_{n+1})$  into  $|01\rangle\langle 01| - |10\rangle\langle 10|$ .

briefly review the variational Hamiltonian ansatz (VHA), [24], which is used to construct the ground state.

The defining idea of VHA is to find a unitary operator  $U(\theta)$ , such that under variations of the parameters  $\theta_i$  from the set  $\theta$  one minimizes the energy expectation value  $\langle \Psi_0 | U^\dagger(\theta) H U(\theta) | \Psi_0 \rangle$ , where  $|\Psi_0\rangle$  is a guess state which can be prepared easily. Identifying an underlying operator  $H$  as the sum of  $p$  independent terms  $H = \sum_{j=1}^p H_j$ , the operator  $U(\theta)$  is defined over  $n$  steps as

$$U(\theta) = \prod_{k=1}^n \prod_{j=1}^p e^{-i\theta_{j,k} H_j}. \quad (17)$$

In each step  $k$ , the  $p$  parameters are updated until energy measurements on  $|\Psi\rangle = U(\theta)|\Psi_0\rangle$  yield minimum values. An example for a rule set governing the update of  $\theta_{j,k}$  can be found in [25].

### C. Measuring ground state energy

Finding the minimum expectation value  $\langle \Psi_0 | U^\dagger(\theta) H U(\theta) | \Psi_0 \rangle$  as pointed out in the previous section requires energy measurements. From Eq. (1) we find terms for hopping and repulsion, which in the following we refer to as  $H_0$  and  $H_U$ , respectively. Hence, schedules for measurement of hopping and repulsion energy, cf. [8], are reviewed.

Measurements of repulsion energy are done by measuring each qubit in the computational basis. Since we operate within the Jordan-Wigner framework, repulsion terms are mapped to the matrix  $|11\rangle\langle 11|_{mn}$ , where  $m, n$  correspond the inspected orbitals belonging to one parent site. Hence, the energy equals the probability to find both qubits to be in state  $|1\rangle$ .

Measurements of kinetic energies depend on the hopping direction, which is rooted in the way how the Jordan-Wigner strings are chosen in the mapping (9). For one of the possible choices, Fig. 18, horizontal hoppings are considered less costly in terms of gate depth since Jordan-Wigner strings can be neglected, whereas vertical hoppings may lead to long Jordan-Wigner strings.

Following [8], horizontal hopping map to the matrix  $\frac{1}{2}(X_n X_{n+1} + Y_n Y_{n+1})$ . In order to perform computational basis measurements, the unitary that diagonalizes  $\frac{1}{2}(X_n X_{n+1} + Y_n Y_{n+1})$  into  $|01\rangle\langle 01| - |10\rangle\langle 10|$  is shown in Fig. 5. Desired energy expectation is thus the probabil-

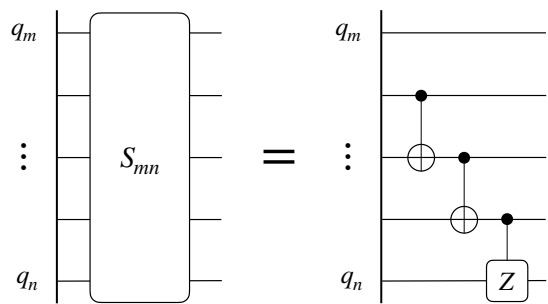


FIG. 6. Definition of the operator  $S_{mn}$ , which purpose is to remove Jordan-Wigner strings. It is non-trivial for  $m - n \geq 2$  and we set  $S_{n+1,n} = \mathbb{1}$ .

ity of measuring  $|01\rangle$  minus the probability of measuring  $|10\rangle$ .

On the other hand, a kinetic energy term  $h_{ij}^{\sigma\sigma'}$  describing vertical hopping is mapped to the operator (14), which contains an additional Jordan-Wigner string. As discussed in subsection III A, the latter can be eliminated by similarity transformation via the unitary  $S_{mn}$  shown in Fig. 6. Afterwards, one can measure two terms in  $h_{ij}^{\sigma\sigma'}$  separately. The quantum circuit to implement the measurement of the first term,  $iy_{i\sigma} x_{j\sigma'}$ , is given in Fig. 7. It is based on the following similarity transformation of this operator, i. e.

$$\begin{aligned} iy_{i\sigma} x_{j\sigma'} &= \mathbf{S}_{mn}^\dagger (Z_m Z_n) \mathbf{S}_{mn}, \\ \mathbf{S}_{mn} &= (H_m H_n) S_{mn}. \end{aligned} \quad (18)$$

The expectation value of this operator is then reduced to the average parity of qubits  $m$  and  $n$ . A measurement of the second term in the hopping term,  $-ix_{i\sigma} y_{j\sigma'}$ , is implemented along the same lines with the only difference that the Hadamard gate is replaced by  $X_{\pi/2}$ .

### D. Green's function measurement

We present two routes to measure the Green's function. The orthodox way goes back to the Hadamard test circuit originally proposed in Ref. [12], see Fig. 8. Another

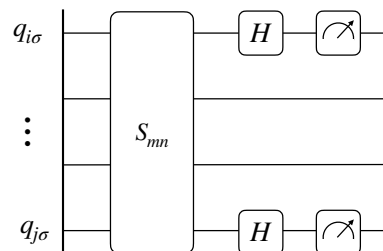


FIG. 7. Measurement of  $iy_{i\sigma} x_{j\sigma}$  term which is reduced to  $\langle Z_{i\sigma} Z_{j\sigma'} \rangle$  after a similarity transformation.

one makes use of linear response theory, particularly the Kubo formula, which we present afterwards.

### 1. The Hadamard test

The Hadamard test is a rather intuitive scheme, which takes into account the perturbation onto a system, as if a particle were taken from the system and added back at a later point in time. The corresponding circuit to evaluate the Green's function is given in Fig. 8. Let  $q_0, \dots, q_3$  be the qubits representing a small physical system and let the last qubit in state  $|0\rangle$  be the control qubit. The first step is to perform a Hadamard operation onto the control qubit. This paves the way for a controlled evolution of the system. The next step is to induce a perturbation to the system, which we denote as  $\sigma_\mu$ , acting on qubit  $q_\mu$ , where  $\sigma_\mu$  may refer to any of the Hermitian Majorana operators  $x_\mu, y_\mu$ . The two  $\sigma$  terms appearing in the circuit shown in Fig. 8 represent a combination of two field operators as given in Eq. (8). As can be seen by the equation, inbetween two ladder operations and after the last, there is the free time evolution denoted by  $U(\tau)$ .

A final Hadamard gate on the control qubit removes the superposition caused by the first Hadamard gate and for time  $\tau$  we measure the correlation function  $g_{\mu\nu}(\tau)$  as

$$\text{Re}(ig_{\mu\nu}(\tau)) = P_{\mu\nu}(\mathcal{M} = 0, \tau) - P_{\mu\nu}(\mathcal{M} = 1, \tau), \quad (19)$$

where  $P_{\mu\nu}(\mathcal{M}, \tau)$  is the empirical probability of measuring  $\mathcal{M}$  at time  $\tau$ .

The Hadamard test circuit requires four blocks of controlled evolution, which include computationally costly two-qubit gates. Gate count comparisons of presented methods are discussed in section V. If the average is performed over the ground state, then one evolution operator can be omitted thereby reducing the amount of gates by a factor of two [26]. For the recent realization of such scheme, we refer to the work [16]. The drawback of this approach is an implicit assumption that the action of an evolution operator on the ground state reduces to the phase,  $U(\tau)|\Psi_0\rangle = |\Psi_0\rangle e^{-iE_0\tau}$ . The latter can be violated for approximate ground states found, e.g., by means of VHA. Not to mention that correlators at out-of-equilibrium remain out of reach.

### 2. Direct measurement

In this subsection we propose an alternative approach to evaluate the Green's function on a quantum computer, which we refer to in what follows as the direct measurement. We will see, that this approach can reduce the depth of the circuit by at least a factor of two. Importantly, it requires no assumption on the initial density matrix  $\rho_0$  of a simulated many-body system and, in contrast with the Hadamard test, relies merely on the

forward uncontrolled evolution operator  $U(\tau)$ . Furthermore, we use the two-site dimer toy model to demonstrate the direct measurement and probe its potential for being a superior method for accessing the system's Green's function.

Exploiting Green's functions for calculating observables and order parameters is motivated by linear response theory (cf. Appendix A). Let  $H'(t) = H + V(t)$  be our system of interest, with  $H$  being the stationary, time-independent part and  $V(t) = \sum_i \Phi_i(t)A_i$  being the time-dependent perturbation, whose exact form we specify momentarily. Linear response theory describes how the system reacts to a given perturbation  $V(t)$ , where  $\Phi_i(t)$  is the interaction strength of operator  $A_i$ . If we assume a sufficiently weak perturbation, the change in an expectation value of any Heisenberg operator  $\tilde{A}_i(t)$  defined relative to the full Hamiltonian  $H'(t)$  is linear in the perturbing source  $\Phi(t)$ . This is formulated as

$$\delta\langle\tilde{A}_i(t)\rangle = \int dt' \chi_{ij}(t; t') \Phi_j(t'), \quad (20)$$

where  $\chi_{ij}(t; t')$  is the response function given by

$$\chi_{ij}(t, t') = -i\theta(t - t')\langle[A_i(t), A_j(t')]\rangle. \quad (21)$$

Here, operators  $A_j(t)$  evolve under the action of the non-perturbed Hamiltonian  $H$  and, as before, is averaged over an initial density matrix  $\rho_0$ . In particular, for the perturbation localized in time at time  $t'$ , one writes  $\Phi_j(t) = \Phi_j \delta(t - t')$ , and arrives at the relation

$$\delta\langle\tilde{A}_i(t)\rangle = \sum_j \chi_{ij}(t; t') \Phi_j. \quad (22)$$

which can be used to extract the response function in the experiment. One assumes here that  $\Phi_j$  is relatively small so that non-linear effects can be disregarded.

To adapt this general idea to the Green's function measurement of  $c$ -fermions in our system, we couple them to an auxiliary spinless  $d$ -fermion with the Hamiltonian  $H_d = \epsilon_d d^\dagger d$  and introduce the hopping operator

$$A_j^\sigma = d^\dagger c_{j\sigma} + c_{j\sigma}^\dagger d \quad (23)$$

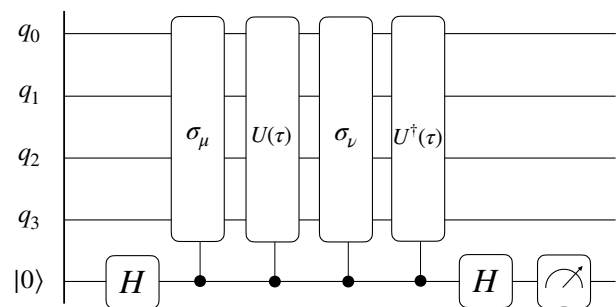


FIG. 8. Quantum circuit for measuring correlation functions  $C_{\mu\nu}$ . The first four qubits  $q_0, \dots, q_3$  represent the physical system, whereas the last qubit in state  $|0\rangle$  represents the control qubit.

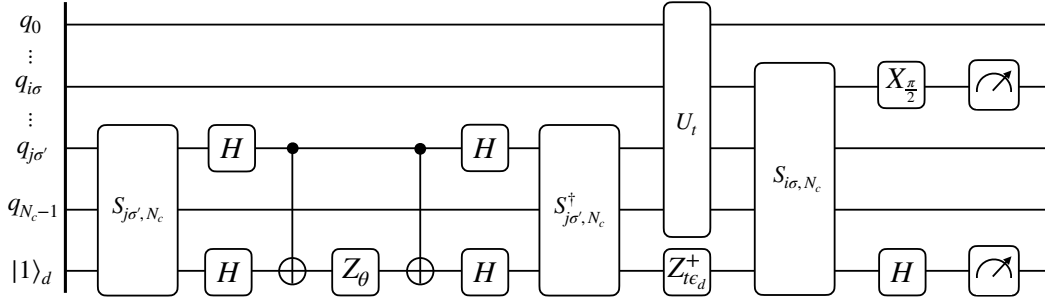


FIG. 9. Measurement of the correlator  $\langle\{x_{i\sigma}(\tau), y_{j\sigma'}(0)\}\rangle$ . The unitary  $U_t$  refers to the Trotterized evolution under the Hubbard cluster Hamiltonian (1). While the  $Z$ -rotation with the angle  $\theta = \Phi_j^{\sigma'}$  is due to perturbation, the  $Z^\dagger$ -rotation with the angle  $t\epsilon_d$  accounts for a free evolution of the  $d$ -fermion.

acting on the  $j$ -th fermion, while the ancilla qubit stores the state of the  $d$ -fermion. The explicit form of the perturbation  $V(t)$  then reads

$$V(t) = \sum_j \Phi_j^\sigma(t) A_j^\sigma = \sum_j \Phi_j^\sigma(t) [d^\dagger c_{j\sigma} + c_{j\sigma}^\dagger d], \quad (24)$$

where again  $\Phi_j^\sigma(t)$  is the external field acting on the  $j$ -th fermion with spin  $\sigma$ . Furthermore, considering the response function (21) we may assume  $t' = 0$  and  $t > t'$  such that we can neglect the  $t'$ -dependence. The commutator then becomes

$$\chi_{ij}^{\sigma\sigma'}(t) = -i \left( \langle A_i^\sigma(t) A_j^{\sigma'} \rangle - \langle A_j^{\sigma'} A_i^\sigma(t) \rangle \right). \quad (25)$$

Using Eq. (23), this leads to

$$\begin{aligned} \chi_{ij}^{\sigma\sigma'}(t) = & -i \langle (d^\dagger(t) c_{i\sigma}(t) + c_{i\sigma}^\dagger(t) d(t)) \cdot (d^\dagger c_{j\sigma'} + c_{j\sigma'}^\dagger d) \rangle \\ & + i \langle (d^\dagger c_{j\sigma'} + c_{j\sigma'}^\dagger d) \cdot (d^\dagger(t) c_{i\sigma}(t) + c_{i\sigma}^\dagger(t) d(t)) \rangle. \end{aligned}$$

If we assume the  $d$ -fermion orbital to be occupied, it follows that  $\langle d^\dagger(t) d \rangle \neq 0$  and  $\langle d(t) d^\dagger \rangle = 0$ . Hence, the above equation simplifies to

$$\chi_{ij}^{\sigma\sigma'}(t) = -i \langle d^\dagger(t) d c_{i\sigma}(t) c_{j\sigma'}^\dagger \rangle + i \langle d^\dagger d(t) c_{j\sigma'} c_{i\sigma}^\dagger(t) \rangle. \quad (26)$$

Wick's theorem can be used to write the four-point correlators in terms of a combination of two-point correlators. The only non-zero two-point correlators are  $\langle d^\dagger(t) d \rangle$ ,  $\langle c_i(t) c_j^\dagger \rangle$ ,  $\langle d^\dagger d(t) \rangle$  and  $\langle c_j c_i^\dagger(t) \rangle$ . It then follows that

$$\chi_{ij}^{\sigma\sigma'}(t) = -i \langle d^\dagger(t) d \rangle \langle c_{i\sigma}(t) c_{j\sigma'}^\dagger \rangle + i \langle d^\dagger d(t) \rangle \langle c_{j\sigma'} c_{i\sigma}^\dagger(t) \rangle, \quad (27)$$

where  $\langle d^\dagger(t) d \rangle$  and  $\langle d^\dagger d(t) \rangle$  equal  $e^{i\epsilon_d t}$  and  $e^{-i\epsilon_d t}$ , respectively. Finally, we arrive at

$$\chi_{ij}^{\sigma\sigma'}(t) = -i e^{i\epsilon_d t} \langle c_{i\sigma}(t) c_{j\sigma'}^\dagger \rangle + i e^{-i\epsilon_d t} \langle c_{j\sigma'} c_{i\sigma}^\dagger(t) \rangle. \quad (28)$$

The above relation can be represented in the equivalent form:

$$\chi_{ij}^{\sigma\sigma'}(t) = \sin \lambda \langle \{c_{i\sigma}(t), c_{j\sigma'}^\dagger\} \rangle - i \cos \lambda \langle [c_{i\sigma}(t), c_{j\sigma'}^\dagger] \rangle, \quad (29)$$

where  $\lambda = \epsilon_d t$ . Since the energy of the  $d$ -fermion  $\epsilon_d$  is quasi-arbitrary, one may vary the phase  $\lambda$  to recover two independent Green's functions. By setting  $\lambda = \pi/2$  one obtains the retarded Green's function given by the anti-commutator, while the choice  $\lambda = 0$  leads to the so-called Keldysh correlator expressed via the commutator of two fermion operators.

When it comes to the actual measurement protocol using the outlined linear response scheme, it is advantageous to perform the measurements in the Majorana basis and use the relation (10) to reconstruct the Green's function of complex fermions afterwards. As an example, let us consider the measurement of the correlator of two Hermitian operators  $x_{i\sigma}(t)$  and  $y_{j\sigma'}$ . To this end we introduce two Majorana fermions,  $x_d = d + d^\dagger$  and  $y_d = i(d - d^\dagger)$ , associated with the auxiliary  $d$ -fermion and define hopping operators as follows, cf. Eq. (13)

$$A_i^\sigma = \frac{i}{2} x_{i\sigma} x_d, \quad A_j^{\sigma'} = \frac{i}{2} y_{j\sigma'} x_d. \quad (30)$$

Repeating the steps leading to the intermediate result (27), one finds that for such choice of hopping operators  $\chi_{ij}^{\sigma\sigma'}(t)$  changes to

$$\begin{aligned} \chi_{ij}^{\sigma\sigma'}(t) = & -\frac{i}{4} \langle x_d(t) x_d \rangle \langle x_{i\sigma}(t) y_{j\sigma'} \rangle \\ & + \frac{i}{4} \langle x_d x_d(t) \rangle \langle y_{j\sigma'} x_{i\sigma}(t) \rangle. \end{aligned} \quad (31)$$

Additionally, the correlator of an auxiliary Majorana fermion becomes  $\langle x_d(t) x_d \rangle = e^{i\epsilon_d t}$ . This means that for the Green's functions of Majorana operators we can use exactly the same final relation (29). In particular, the retarded correlator reads

$$\frac{1}{4} \langle \{x_{i\sigma}(t), y_{j\sigma'}\} \rangle = \chi_{ij}^{\sigma\sigma'}(t) \Big|_{\epsilon_d t = \pi/2}. \quad (32)$$

For the later purpose it is advantageous to rewrite the above relation as

$$\frac{1}{2} \langle \{x_{i\sigma}(t), y_{j\sigma'}\} \rangle = \frac{\langle i x_{i\sigma} x_d \rangle \Phi(t, \epsilon_d)}{\sin \Phi_j^{\sigma'}} \Big|_{\epsilon_d t = \pi/2}, \quad (33)$$

where  $\langle \dots \rangle_{\Phi}$  refers to an average in the presence of a perturbation. Note, that within the linear response theory framework the denominator needs to be substituted by just  $\Phi_j^{\sigma'}$ . In this case the relation (33) follows from Eqs. (22) and (32), where  $\langle A_i^{\sigma} \rangle = \frac{i}{2} \langle i x_{i\sigma} x_d \rangle_{\Phi}$  and we took into account that  $\langle A_i^{\sigma} \rangle$  vanishes in the absence of perturbation. In Appendix B we evaluate the response  $\langle A_i^{\sigma} \rangle$  to the source field in all orders and prove the validity of Eq. (33) at arbitrary  $\Phi_j^{\sigma'}$ .

We are now in a position to present the quantum circuit (see Fig. 9), which accomplishes the measurement of the correlator (33). It can be rationalized as follows. Right after the initialization of a quantum computer to the ground state with the help of VHA (not shown) one applies the perturbation with the potential  $V(t)$ . It can be achieved in one Trotter step yielding the unitary

$$\exp\left(\frac{1}{2}\Phi_j^{\sigma'} y_{j\sigma'} x_d\right) = S_{j\sigma', N_c}^{\dagger} \exp\left(-\frac{i}{2}\Phi_j^{\sigma'} X_{j\sigma'} X_{N_c}\right) S_{j\sigma', N_c}. \quad (34)$$

Its circuit representation is analogous to the one describing the evolution under the hopping term, see Fig. 3. In this context, it entangles the ancilla qubit used to represent the  $d$ -fermion with the qubits' states representing the cluster. Subsequent independent evolutions of the cluster and the  $d$ -fermion are then followed by the measurement of an operator  $A_i^{\sigma} = \frac{i}{2} x_{i\sigma} x_d$ . The way to average such operator has already been described in subsection III C: in a few unitary transformations  $\langle A_i^{\sigma} \rangle$  can be related to the average parity of two qubits,  $\langle Z_{i\sigma} Z_{N_c} \rangle$ , see Fig. 7.

Our primary focus in this paper is on the retarded Green's function given by the anti-commutator (33), since the latter eventually enters into the VCA scheme outlined in Sec. II. However, the full set of possible Green's functions can be evaluated using the proposed algorithm. For instance, for the Keldysh correlator of Majoranas one can write

$$-\frac{i}{2} \langle [x_{i\sigma}(t), y_{j\sigma'}] \rangle = \left. \frac{\langle i x_{i\sigma} x_d \rangle_{\Phi}(t, \epsilon_d)}{\sin \Phi_j^{\sigma'}} \right|_{\epsilon_d=0}, \quad (35)$$

Then other correlators, such as  $g_{ij}^{\sigma\sigma'}(t)$  defined in Eq. (11), can be reconstructed from the retarded and Keldysh Green's functions. Additionally, the best choice for the strength of the perturbation is  $\Phi_j^{\sigma'} = \pi/2$ , which leads to the strongest response and is used for quantum computations in what follows.

#### IV. TWO-SITE DIMER MODEL

In this section we introduce a two-site dimer [27] that serves as our toy model for which we evaluate the Green's function. Following the general framework outlined in Sec. II, it can be seen as the smallest non-trivial cluster, so that the variational cluster approximation is able to

deliver physically reasonable results. Specifically, within VCA such minimal cluster is sufficient to reproduce the Mott insulating transition in the Hubbard model. On the other hand, in order to recover the d-wave superconducting phase, one needs at least four sites per cluster [28].

The two-site dimer model consists of a Hubbard site that is coupled to a bath site. Its Hamiltonian at half-filling given by

$$H' = H_0 + H_U = -t \sum_{\sigma} (c_{\sigma}^{\dagger} b_{\sigma} + b_{\sigma}^{\dagger} c_{\sigma}) + \frac{U}{2} (n_c^2 - 2n_c), \quad (36)$$

where  $t$  is the hopping energy and  $U$  is the Coulomb repulsion. The field operators  $c_{\sigma}^{\dagger}, c_{\sigma}$  respectively creates or destroys a fermion with spin  $\sigma$  at the Hubbard site, while  $b_{\sigma}^{\dagger}, b_{\sigma}$  respectively creates or destroys a fermion with spin  $\sigma$  at the bath site and  $n_c = \sum_{\sigma} c_{\sigma}^{\dagger} c_{\sigma}$ . Lastly, the linear  $n_c$  term in  $H_U$  stems from a chemical potential  $\mu = U$  at half-filling.

Qubit ordering is shown in Fig. 10 and is chosen in a way that allows for decreasing circuit depth, see section IV A.

Investigating the dimer at half-filling allows us to concentrate on just six out of 16 possible state configurations. With  $|0\rangle$  being the vacuum state, following states  $|1\rangle, |2\rangle, \dots, |6\rangle$  are possible as two electrons reside at the dimer:

$$\begin{aligned} |1\rangle &= c_{\downarrow}^{\dagger} c_{\uparrow}^{\dagger} |0\rangle, & |2\rangle &= c_{\uparrow}^{\dagger} b_{\uparrow}^{\dagger} |0\rangle, & |3\rangle &= b_{\downarrow}^{\dagger} b_{\uparrow}^{\dagger} |0\rangle \\ |4\rangle &= b_{\downarrow}^{\dagger} c_{\uparrow}^{\dagger} |0\rangle, & |5\rangle &= b_{\uparrow}^{\dagger} c_{\uparrow}^{\dagger} |0\rangle, & |6\rangle &= b_{\downarrow}^{\dagger} c_{\downarrow}^{\dagger} |0\rangle. \end{aligned} \quad (37)$$

In matrix form, the Hamiltonian (36) thus reads

$$H' = - \begin{pmatrix} 0 & -t & 0 & t & 0 & 0 \\ -t & \frac{U}{2} & -t & 0 & 0 & 0 \\ 0 & -t & 0 & t & 0 & 0 \\ t & 0 & t & \frac{U}{2} & 0 & 0 \\ 0 & 0 & 0 & 0 & \frac{U}{2} & 0 \\ 0 & 0 & 0 & 0 & 0 & \frac{U}{2} \end{pmatrix}, \quad (38)$$

with the ground state energy

$$E_0 = -\frac{1}{4} (U + \sqrt{U^2 + 64t^2}), \quad (39)$$

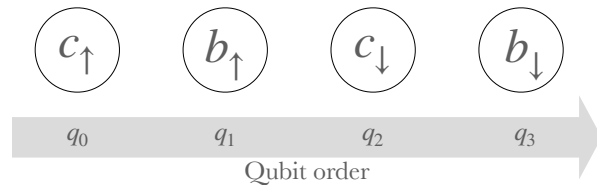


FIG. 10. Indexing qubits over two Hubbard sites and two bath sites.



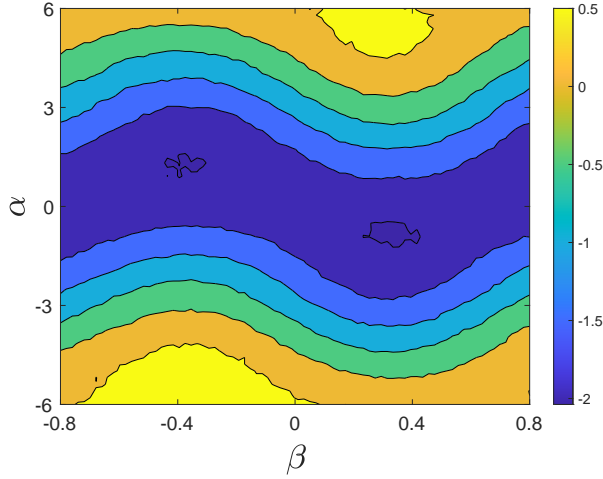


FIG. 11. (Color online). Energy landscape for the two-site dimer for finding its ground state via the variational Hamiltonian ansatz with angles  $\alpha$  and  $\beta$  shown for  $t = 1$  and  $U = 4$ . Resulting energies were evaluated on the *ibmq\_quito* chip, an open-access IBM-Q quantum superconducting device, with the optimum lying very close to theoretical values  $\alpha_* = -0.92$  and  $\beta_* = 0.39$  found from Eq. (47).

corresponding to the eigenstate

$$|\Psi\rangle \propto C(|1\rangle + |3\rangle) + |2\rangle + |4\rangle, \quad C = \frac{\sqrt{U^2 + 64t^2} - U}{8t}, \quad (40)$$

up to a normalization factor. Lastly, we find the expectation values of  $H_0$  and  $H_U$  to be

$$\langle H_0 \rangle = -\frac{U}{4} \left( 1 + \frac{U}{\sqrt{U^2 + 64t^2}} \right) \quad (41)$$

and

$$\langle H_U \rangle = -\frac{16t^2}{\sqrt{U^2 + 64t^2}}. \quad (42)$$

As required by linear response theory, we need to start from an equilibrium state, i. e. the ground state. Consequently, we present a route to find the ground state via the variational Hamiltonian ansatz (VHA).

### A. Ground state preparation

For the sake of finding the ground state of the dimer system, we employ a technique known as the variational Hamiltonian ansatz [24]. Starting from the ground state of the cluster  $|\Psi_0\rangle$  in the non-interacting limit  $U = 0$ , we aim to find the interacting system's ground state  $|\Psi\rangle$  as

$$|\Psi(\alpha, \beta)\rangle = \prod_{j=1}^p e^{i\beta_j H_0^{t \rightarrow 1}} e^{-i\alpha_j H_U^{U \rightarrow 1}} |\Psi_0\rangle \quad (43)$$

where  $\alpha_j, \beta_j \in \mathbb{R}$  are the variational parameters. The ground state  $|\Psi_0\rangle$  is a Slater determinant. For instance,

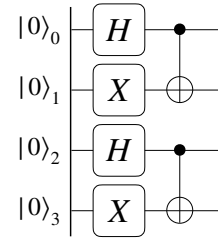


FIG. 12. Quantum circuit to prepare a Slater determinant as a trial Ansatz for the VHA.

Eq. (40) at  $U = 0$  can be written in terms of two  $f$ -fermions,

$$|\Psi_0\rangle = f_\downarrow^\dagger f_\uparrow^\dagger |0\rangle, \quad f_\sigma^\dagger = \frac{1}{\sqrt{2}}(c_\sigma^\dagger + b_\sigma^\dagger), \quad (44)$$

which are linear superpositions of  $b$  and  $c$ .

An initialization of the quantum chip in a Slater determinant state most generally can be constructed from an initial one,  $|0, 0, \dots, 0\rangle$ , by the so-called Given's rotations, [9]. However, for the two-fermion state (44) a much simpler circuit is sufficient. One can verify by direct inspection that the circuit shown in Fig. 12 transforms the vacuum state into  $|\Psi_0\rangle$ . Moreover, it is possible to find the exact matching between the trial and actual ground state functions already for the minimal depth VHA, i.e with  $p = 1$ . Therefore, we find the full circuit to prepare the ground state is a single sequence of the circuit shown in Fig. 12, followed by a variation of the hopping circuit, cf. Fig. 3 and finalized by a simpler variation of the repulsion circuit, Fig. 4.

At this point we note that the evolution operator over a time step  $\Delta\tau$  under the interaction Hamiltonian  $H_U$ , see Eq. (36), reads

$$U(\theta) = \text{CNOT}^{(13)} \cdot R_z^{(3)}(\theta/2) \cdot \text{CNOT}^{(13)}, \quad (45)$$

with angle  $\theta = U \cdot \Delta\tau$ . A difference from the repulsion circuit on Fig. 4 comes from the extra term  $Un_c$  in the present choice of  $H_U$ , which effectively leads to the reduction of two single-qubit  $Z$ -rotation gates. Furthermore, if one of the natural two-qubit gates on the hardware is a controlled-phase gate,  $\text{CT}(\theta)$ , then the unitary (45) can be simplified to

$$U(\theta) = R_z^{(1)}(\theta/2) \cdot R_z^{(3)}(\theta/2) \cdot \text{CT}^{(13)}(-\theta), \quad (46)$$

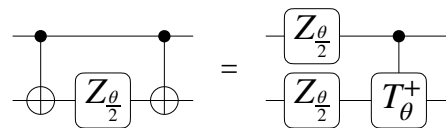


FIG. 13. Circuit identity as used in the two-site dimer.

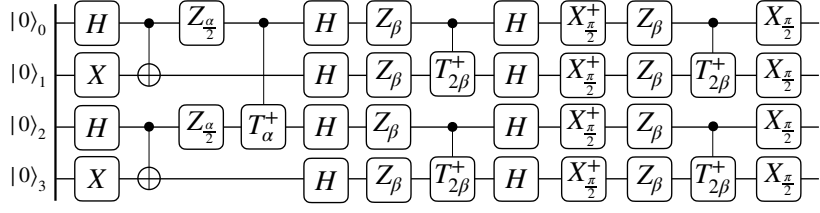


FIG. 14. Reduced quantum circuit for finding the ground state of a correlated system. At the end of the circuit we are left with the interacting ground state of the two-site dimer.

up to a global phase. The equivalence of the two circuits in Eqs. (45) and (46) for  $U(\theta)$  is presented in Fig. 13.

The full circuit to prepare the VHA ground state is presented in Fig. 14. Comparing Fig. 14 to Fig. 4 and 3, we reach a reduction of two two-qubit gates for the repulsion compared to the scheme in Fig. 4 and another reduction of eight two-qubit gates for the new hopping scheme. Finally, the variational energy reads

$$E(\alpha, \beta) = -2t \cos \frac{\alpha}{2} - \frac{U}{4} \left( 1 - \sin \frac{\alpha}{2} \sin 4\beta \right), \quad (47)$$

which depends on just two parameters,  $\alpha$  and  $\beta$ . Fig. 11 shows the corresponding energy landscape.

### B. Analytical formulae for the Green's function

Next we discuss the analytical results for the Green's functions of the two-site model in order to benchmark them with our circuit simulations which we review in the next subsection. Following the ordering of fermion states under Jordan-Wigner mapping shown in Fig. 10, we introduce a set of eight Majorana operators  $\{x_n, y_n\}$  so that

$$\begin{aligned} c_{\uparrow} &= \frac{1}{2}(x_0 - iy_0), & b_{\uparrow} &= \frac{1}{2}(x_1 - iy_1), \\ c_{\downarrow} &= \frac{1}{2}(x_2 - iy_2), & b_{\downarrow} &= \frac{1}{2}(x_3 - iy_3), \end{aligned} \quad (48)$$

with  $n$  being a composite index accounting for both site and spin. Correlation functions of interest take the form given by Eqs. (10) and (11). Because of spin symmetry we find them to be block-diagonal w.r.t. spin indices,

$$ig^{\uparrow\uparrow}(\tau) = \begin{pmatrix} \langle x_0(\tau)x_0(0) \rangle & \langle x_0(\tau)y_1(0) \rangle \\ \langle y_1(\tau)x_0(0) \rangle & \langle y_1(\tau)y_1(0) \rangle \end{pmatrix}, \quad (49)$$

and

$$ig^{\downarrow\downarrow}(\tau) = \begin{pmatrix} \langle x_2(\tau)x_2(0) \rangle & \langle x_2(\tau)y_3(0) \rangle \\ \langle y_3(\tau)x_2(0) \rangle & \langle y_3(\tau)y_3(0) \rangle \end{pmatrix}, \quad (50)$$

with two blocks being mutually equal,  $g^{\uparrow\uparrow}(\tau) = g^{\downarrow\downarrow}(\tau)$ . Other non-zero correlators follow from the symmetries

$$\begin{aligned} \langle x_i(\tau)x_i(0) \rangle &= \langle y_i(\tau)y_i(0) \rangle, & \forall i \\ \langle x_i(\tau)y_{i+1}(0) \rangle &= \langle x_{i+1}(\tau)y_i(0) \rangle, & i = 0, 2. \end{aligned} \quad (51)$$

Additionally, the self-adjoint property of Majorana operators implies that

$$\langle x_i(\tau)y_j(0) \rangle^* = \langle y_j(0)x_i(\tau) \rangle, \quad (52)$$

and the same for  $x-x$  and  $y-y$  correlators. Therefore, the retarded correlator reads

$$\langle \{x_i(\tau), y_j(0)\} \rangle = 2\text{Re} \langle x_i(\tau)y_j(0) \rangle, \quad \tau > 0. \quad (53)$$

We can evaluate the above correlation functions exactly using the Lehmann representation. Starting from  $iG^>(t) = \langle 0|U^\dagger(t)x_iU(t)y_j|0\rangle$ , where  $|0\rangle$  is the ground state, we use the eigenstate decomposition of the evolution operator,  $U(t) = \sum_m^{2^D} |m\rangle e^{-iE_m t} \langle m|$ , with  $D = 4^{N_c}$  being the Hilbert space dimension of a cluster. It then follows that  $iG^>(t) = \sum_m^D e^{-iE_0 t} \langle 0|x_i|m\rangle e^{-iE_m t} \langle m|y_j|0\rangle$ . The eigenstates  $|m\rangle$  can be obtained by exact diagonalization of  $H'$ , cf. Eq. (36), which renders the two-site dimer Green's function amenable to analytic treatment. The correlation functions evaluated in this manner read

$$\begin{aligned} \langle x_0(\tau)x_0(0) \rangle &= \\ e^{-\frac{i}{4}\tau U_2} &\left( \cos \frac{\tau U_1}{4} - \frac{i(U^2 - 32t^2)}{U_1 U_2} \sin \frac{\tau U_1}{4} \right), \end{aligned} \quad (54)$$

$$\begin{aligned} \langle x_1(\tau)x_1(0) \rangle &= \\ e^{-\frac{i}{4}\tau U_2} &\left( \cos \frac{\tau U_1}{4} + \frac{i(U^2 + 32t^2)}{U_1 U_2} \sin \frac{\tau U_1}{4} \right) \end{aligned} \quad (55)$$

and

$$\begin{aligned} \langle x_0(\tau)y_1(0) \rangle &= \\ 4e^{-\frac{i}{4}\tau U_2} &\left( \frac{2it}{U_2} \cos \frac{\tau U_1}{4} - \frac{t}{U_1} \sin \frac{\tau U_1}{4} \right), \end{aligned} \quad (56)$$

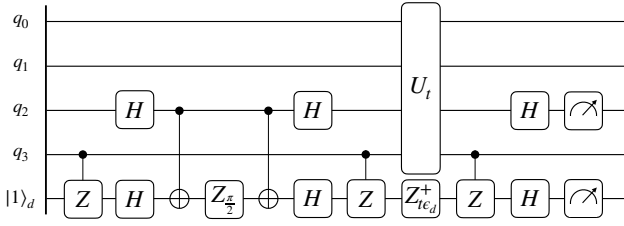
where two additional energy scales,

$$U_1 = \sqrt{U^2 + 16t^2}, \quad U_2 = \sqrt{U^2 + 64t^2}, \quad (57)$$

were introduced to shorten the results.

### C. Quantum circuits for direct measurement of the two-site dimer Green's function

In accordance to section IIID2, we provide quantum circuits for the direct measurement of the Green's function. The  $y_2 - y_2$  correlator is directly measured when

FIG. 15. Circuit for evaluating the  $\langle\{y_2(\tau), y_2(0)\}\rangle$  correlator.

employing the circuit shown in Fig. 15. In turn, circuits for measuring  $y_3-y_3$  and  $y_3-x_2$  correlators are shown in Fig. 16 and Fig. 17, respectively. To implement the unitary evolution operator,  $U_t$ , one applies the Trotterization scheme with a duration of a single step being  $\Delta\tau$ . The one-step evolution operator can be constructed following the same sequence of gates used in VHA circuit, see Fig. 11, with angles  $\alpha = U\Delta\tau$  and  $\beta = -t\Delta\tau$ .

## V. GATE COUNT

We present the exact gate count for an arbitrarily sized cluster in up to three dimensions. Investigating scaling behaviors, one typically is interested in the worst case scenarios. Due to Jordan-Wigner strings, we arrive at maximum gate counts when there is hopping between two orbitals, which - despite being nearest neighbors - expose the maximum distance from each other. The largest distance between two neighbored orbitals in three dimensions is shown in Fig. 18.

### A. Time evolution

As can be seen from Fig. 14, hopping and repulsion terms between two orbitals require a set of one- and two-qubit gates, for which the cardinal numbers are given in Table II, Table III, Table IV (hopping) and Table V (repulsion). Note that half-filling forces the particle number  $N$  to be equal to the total number of dimers. We find  $N_1 = n_x$  in 1D,  $N_2 = n_x n_y$  in 2D and finally  $N_3 = n_x n_y n_z$  in 3D.

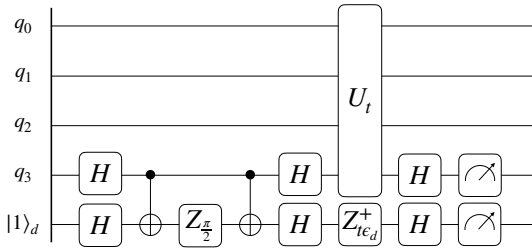
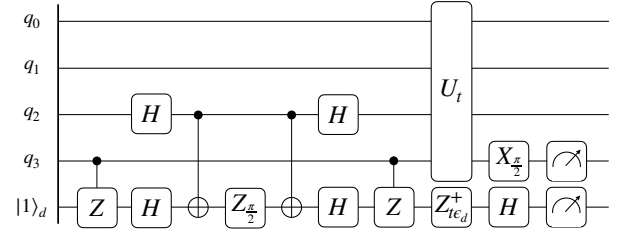
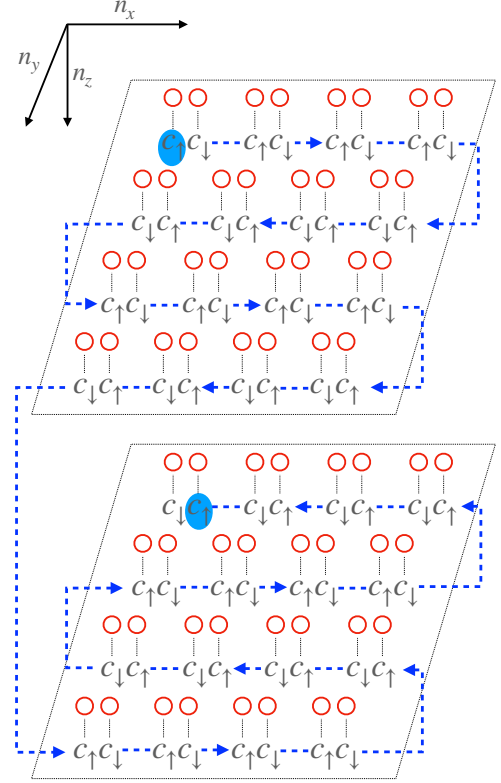
FIG. 16. Circuit for evaluating the  $\langle\{y_3(\tau), y_3(0)\}\rangle$  correlator.FIG. 17. Circuit for evaluating the  $\langle\{x_3(\tau), y_2(0)\}\rangle$  correlator.

FIG. 18. (Color online). Worst case hopping between two neighbored orbitals (highlighted in blue ovals) in 3D with maximum distance from each other. The dashed blue line is the route which gives rise to the longest Jordan-Wigner string. Note, that in general there are more than one of such routes. Red circles represent a heat bath, which is coupled to the corresponding  $c$ -fermion. Coordinate numbers  $n_x, n_y, n_z$  count the number of dimers in  $x, y, z$ -direction. Here:  $n_x = 4, n_y = 4, n_z = 2$ .

### B. Complete evaluation of the dimer Green's function

For a direct comparison of full evaluation gate counts, we discard ground state preparation as it is similar in both cases. Within the Hadamard test, cf. Fig. 8, there is an ancilla control qubit, which in principle elevates all one-qubit gates to two-qubit gates and two-qubit gates to three-qubit gates. However, it is sufficient to only control rotation gates as well as phase gates: If the ancilla

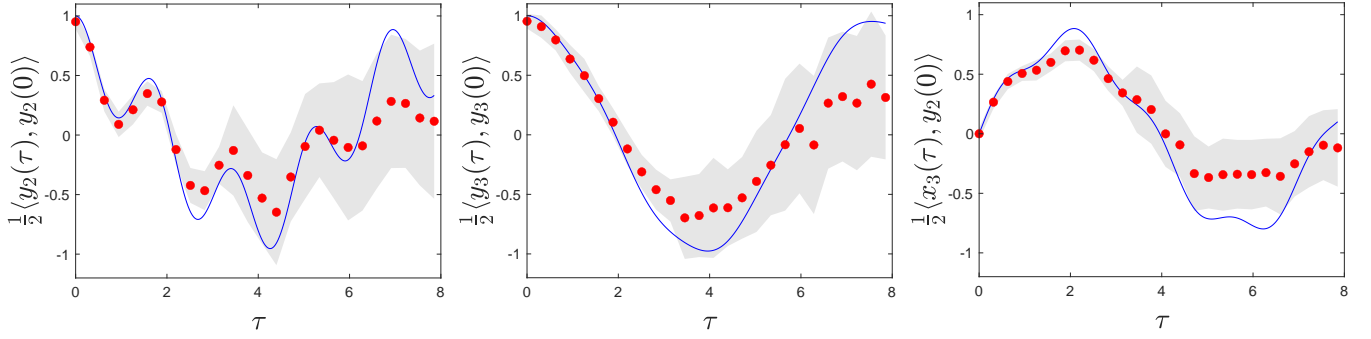


FIG. 19. (Color online.) Correlators  $y_2 - y_2$ ,  $y_3 - y_3$  and  $x_3 - y_2$  evaluated in 25 Trotter steps (red dots) of the duration  $\Delta\tau = 0.314$ . A shaded area (grey) indicates the standard deviation over 100 experiments. The solid blue curves correspond to the analytical results, cf. Eqs. (54–56), where we account for the symmetry relations (51). System parameters are chosen to be  $V = 1$  and  $U = 4V$ . The correlators were evaluated on Qiskit’s noisy *AerSimulator* of the *ibmq.kolkataV2* backend, an open-access simulator of the corresponding IBM-Q superconducting device. Error-mitigating techniques used were measurement calibration (Qiskit), zero-noise extrapolation (Mitiq, [29]) and post-selection of valid measurement results.

	$x$	$y$	$z$	bath
1D	$2(n_x - 1)$	0	0	$2n_x$
2D	$2(n_x - 1)n_y$	$2(n_y - 1)n_x$	0	$2n_x n_y$
3D	$2(n_x - 1)n_y n_z$	$2(n_y - 1)n_x n_z$	$2n_x n_y (n_z - 1)$	$2n_x n_y n_z$

TABLE II. Number of hopping terms for one, two and three dimensions with respect to hopping in  $x, y, z$  direction plus bath hopping. The numbers  $n_x, n_y, n_z$  refer to the amount of dimers in  $x, y, z$  direction, respectively.

	Worst case length of JW-string
1D	$2 \cdot \text{CZ}$
2D	$8(n_x - 1) \cdot \text{CNOT} + 2 \cdot \text{CZ}$
3D	$8(n_x n_y - 1) \cdot \text{CNOT} + 2 \cdot \text{CZ}$

TABLE III. Depth of the worst case operator  $S_{mn}$  corresponding to the Jordan-Wigner string with longest distance between two neighboring qubits, cf. Fig. 18. The numbers  $n_x, n_y$  refer to the amount of dimers in  $x, y$  direction, respectively.

	1-qubit	2-qubit gates	longest JW-string
1D	12	2	2
2D	12	2	$8(n_x - 1) + 2$
3D	12	2	$8(n_x n_y - 1) + 2$

TABLE IV. Gate counts per hopping term for one, two and three dimensions with respect to hopping in  $x, y, z$  direction plus bath hopping. The numbers  $n_x, n_y, n_z$  refer to the amount of dimers in  $x, y, z$  direction, respectively.

	# repulsion terms	1-qubit	2-qubit
1D	$n_x$	2	1
2D	$n_x n_y$	2	1
3D	$n_x n_y n_z$	2	1

TABLE V. Gate counts per repulsion term for one, two and three dimensions. The numbers  $n_x, n_y, n_z$  refer to the amount of dimers in  $x, y, z$  direction, respectively.

	1-qubit	2-qubit	3-qubit
The Hadamard test	$2 + 16 \cdot n_{\Delta\tau}$	$2 + 10 \cdot n_{\Delta\tau}$	$5 \cdot n_{\Delta\tau}$
Direct measurement	$9 + 26 \cdot n_{\Delta\tau}$	$5 + 5 \cdot n_{\Delta\tau}$	0

TABLE VI. Comparison of gate counts for the Hadamard test and direct measurement scheme for the two-site dimer in terms of single qubit, 2-qubit and 3-qubit gates.  $n_{\Delta\tau}$ , number of Trotter steps.

qubit was in the zero state, rotation and phase gates are deactivated, while the action of Hadamard and Y-basis change gates is effectively cancelled out.

For the direct measurement scheme, we focus on the  $y_2 - y_2$  correlator for quantification of circuit metrics, cf. Fig. 15, as it has a larger gate count than the  $x_3 - y_2$  and  $y_3 - y_3$  correlators. One major advantage compared to the Hadamard test lies in the time evolution unitary not being controlled. In Tab. VI we see the direct comparison of the full gate count needed to evaluate the Green’s function of a dimer.

## VI. RESULTS AND DISCUSSION

We show data points for the Green’s function after 25 Trotter steps and plot these against the analytical Green’s function, see Eqs. (54–56). The chosen parameters are  $V = 1$ ,  $U = 4V$ ,  $\Phi = \pi/2$  and  $\epsilon_{dt} = \pi/2$ .

It can be seen, that 25 Trotter steps are sufficient to have a decent overlap of measurement points and the analytic correlator up to time  $\tau \sim 8$ . Single-qubit gates take typical operation times of 20ns, two- and three-qubit gates may be designed with operation times of typically 100ns. It is thus crucial to reduce two- and multi-qubit gates as much as possible to keep operation time small and quantum state fidelity large.

From Tab. VI we see an improvement of factor  $\sim 3$  in terms of multi-qubit gates with respect to the direct

measurement scheme. We further report a rise in one-qubit gates of  $< 62\%$ . Since multi-qubit gates take 5 times as long, the increase in operation time due to a rise in single-qubit gates is suppressed by the decrease in two-qubit gates, which have a larger impact on the total operation time.

Finally, we have presented a quantum algorithm that is based on linear response to evaluate the Green's function on a quantum computer. The number of required measurements scales polynomially in the number of sites  $N_c$  within the cluster and the number of qubits scales linearly in  $N_c$ . The new algorithm is superior in terms of two-qubit gates as well as operation time when compared to the Hadamard test. For a large number of Trotter steps,  $n_{\Delta\tau}$ , we report an improvement factor of  $\sim 1.8$  in gate operation time. Directly measuring the Green's function

is thus an alternative to the Hadamard test and has the potential to outperform the latter in terms of gate count, operation time and thereby fidelity of measured quantities.

## ACKNOWLEDGEMENTS

The authors gratefully acknowledge funding, support and computational resources from Mercedes-Benz AG. We further acknowledge support from OpenSuperQ-Plus100 (101113946) and German Federal Ministry of Education and Research in the funding program "Quantum technologies – from basic research to market", contract number 13N15584 (DAQC). Furthermore, we acknowledge useful conversations with Clemens Possel.

- 
- [1] E. Dagotto, Correlated electrons in high-temperature superconductors, *Reviews of Modern Physics* **66**, 763 (1994).
- [2] G. Moeller, Q. Si, G. Kotliar, M. Rozenberg, and D. S. Fisher, Critical behavior near the Mott transition in the Hubbard model, *Physical Review Letters* **74**, 2082 (1995).
- [3] E. Y. Andrei and A. H. MacDonald, Graphene bilayers with a twist, *Nature Materials* **19**, 1265 (2020).
- [4] I. Siddiqi, Engineering high-coherence superconducting qubits, *Nature Reviews Materials* **6**, 875 (2021).
- [5] Y. S. Meng and M. E. Arroyo-de Dompablo, First principles computational materials design for energy storage materials in lithium ion batteries, *Energy Environ. Sci.* **2**, 589 (2009).
- [6] J. Hubbard, Electron correlations in narrow energy bands, *Proceedings of the Royal Society of London. Series A. Mathematical and Physical Sciences* **276**, 238 (1963).
- [7] F. Arute, K. Arya, R. Babbush, D. Bacon, J. Bardin, R. Barends, R. Biswas, S. Boixo, F. Brandao, D. Buell, B. Burkett, Y. Chen, Z. Chen, B. Chiaro, R. Collins, W. Courtney, A. Dunsworth, E. Farhi, B. Foxen, and J. Martinis, Quantum supremacy using a programmable superconducting processor, *Nature* **574**, 505 (2019).
- [8] C. Cade, L. Mineh, A. Montanaro, and S. Stanisic, Strategies for solving the Fermi-Hubbard model on near-term quantum computers, *Phys. Rev. B* **102**, 235122 (2020).
- [9] D. Wecker, M. B. Hastings, N. Wiebe, B. K. Clark, C. Nayak, and M. Troyer, Solving strongly correlated electron models on a quantum computer, *Phys. Rev. A* **92**, 062318 (2015).
- [10] D. Sénéchal, D. Perez, and D. Plouffe, Cluster perturbation theory for Hubbard models, *Phys. Rev. B* **66**, 075129 (2002).
- [11] M. Potthoff, Self-energy-functional approach to systems of correlated electrons, *European Physical Journal B* **32**, 429 (2003).
- [12] R. Somma, G. Ortiz, J. E. Gubernatis, E. Knill, and R. Laflamme, Simulating physical phenomena by quantum networks, *Phys. Rev. A* **65**, 042323 (2002).
- [13] P.-L. Dallaire-Demers and F. K. Wilhelm, Method to efficiently simulate the thermodynamic properties of the Fermi-Hubbard model on a quantum computer, *Phys. Rev. A* **93**, 032303 (2016).
- [14] P.-L. Dallaire-Demers and F. K. Wilhelm, Quantum gates and architecture for the quantum simulation of the Fermi-Hubbard model, *Phys. Rev. A* **94**, 062304 (2016).
- [15] B. Bauer, D. Wecker, A. J. Millis, M. B. Hastings, and M. Troyer, Hybrid quantum-classical approach to correlated materials, *Phys. Rev. X* **6**, 031045 (2016).
- [16] F. Libbi, J. Rizzo, F. Tacchino, N. Marzari, and I. Tavernelli, Effective calculation of the Green's function in the time domain on near-term quantum processors, *Phys. Rev. Res.* **4**, 043038 (2022).
- [17] A. Altland and B. D. Simons, *Condensed Matter Field Theory*, 2nd ed. (Cambridge University Press, 2010).
- [18] C. V. Raman and K. S. Krishnan, A new type of secondary radiation, *Nature* **121**, 501 (1928).
- [19] D. J. Thouless, Electrons in disordered systems and the theory of localization, *Physics Reports* **13**, 93 (1974).
- [20] J. Hubbard, Electron correlations in narrow energy bands, *Proc. R. Soc. Lond. A* **276**, 238 (1963).
- [21] J. M. Luttinger and J. C. Ward, Ground-state energy of a many-fermion system. II, *Physical Review* **118**, 1417 (1960).
- [22] One exception is the so-called SYK model with random all-to-all two-body interaction, where the Luttinger functional can be found on average,  $\Phi[\mathbf{G}] = J \int d^2\tau G_{\tau_1\tau_2}^4$ , with  $J$  being an interaction strength.
- [23] Y. Gu, A. Kitaev, S. Sachdev, and G. Tarnopolsky, Notes on the complex Sachdev-Ye-Kitaev model, *Journal of High Energy Physics* **2020**, 10.1007/jhep02(2020)157 (2020).
- [24] J.-M. Reiner, F. Wilhelm-Mauch, G. Schön, and M. Marthaler, Finding the ground state of the Hubbard model by variational methods on a quantum computer with gate errors, *Quantum Science and Technology* **4**, 035005 (2019).
- [25] T. Piskor, J.-M. Reiner, S. Zanker, N. Vogt, M. Marthaler, F. K. Wilhelm, and F. G. Eich, Using gradient-based algorithms to determine ground-state energies on a quantum computer, *Phys. Rev. A* **105**, 062415 (2022).

(2022).

- [26] One can also argue that it suffices to control only measured unitary operators  $\sigma$ , while forward and backward evolution operators can be left uncontrolled [9]. Such simplification however is based on the identity  $U(\tau)U^\dagger(\tau) = \mathbb{1}$  which tends to be violated in the case of NISQ devices at long experimental times.
- [27] R. Eder, The Variational Cluster Approximation, in *Emergent Phenomena in Correlated Matter, Modeling and Simulation*, Vol. 3, edited by E. Pavarini, E. Koch, and U. Schollwöck (Verlag des Forschungszentrum Jülich, 2013) Chap. 4.
- [28] D. Sénéchal, An introduction to quantum cluster methods (2010), [arXiv:0806.2690](https://arxiv.org/abs/0806.2690) [cond-mat.str-el].
- [29] R. LaRose, A. Mari, S. Kaiser, P. J. Karalekas, A. A. Alves, P. Czarnik, M. E. Mandouh, M. H. Gordon, Y. Hindy, A. Robertson, P. Thakre, M. Wahl, D. Samuel, R. Mistri, M. Tremblay, N. Gardner, N. T. Stemen, N. Shammah, and W. J. Zeng, Mitiq: A software package for error mitigation on noisy quantum computers, *Quantum* **6**, 774 (2022).

## Appendix A: Derivation of the Kubo formula

In this Appendix we summarize the basics of linear response theory and derive the generalized susceptibility (25). Consider the Hamiltonian of a system,  $H'(t) = H + V(t)$ , with a perturbation  $V(t) = \sum_j \Phi_j(t) A_j$  acting at times  $t > 0$  and given by the sum of hopping operators  $A_j$  defined in Eq. (23). Let also  $\rho_0 = \rho(t = 0)$  be an initial density matrix. Presently, we have  $\rho_0 = |\Psi(\alpha_*, \beta_*)\rangle\langle\Psi(\alpha_*, \beta_*)|$ , with  $(\alpha_*, \beta_*)$  being the optimal parameters of the VHA. However the exact form of  $\rho_0$  is not important for what follows.

By introducing the Heisenberg operators,  $\tilde{A}_i(t) = e^{iH't} A_i e^{-iH't}$ , we are aiming to find how their averages,

$$\langle \tilde{A}_i(t) \rangle_\Phi = \text{tr}(\rho_0 A_i(t)), \quad (\text{A1})$$

change in time in response to the perturbation  $V(t)$ . Here, a subscript in the average,  $\langle \dots \rangle_\Phi$ , indicates that the latter is a functional of generalized forces  $\Phi_j(t)$ . To this end, we switch to the interaction picture by defining  $A_i(t) = e^{iHt} A_i e^{-iHt}$  such that the average in Eq. A1 becomes

$$\langle \tilde{A}_i(t) \rangle_\Phi = \text{tr}[\rho_0 U^\dagger(t) A_i(t) U(t)], \quad (\text{A2})$$

where

$$U(t) = e^{iHt} e^{-iH't} \equiv T_t \exp \left\{ -i \int_0^t V_I(t') dt' \right\} \quad (\text{A3})$$

is an evolution operator in the interaction picture expressed via  $V_I(t) = \sum_j \Phi_j(t) A_j(t)$ . At this point we may expand  $U(t)$  up to first order in perturbation  $V_I(t)$  and obtain

$$\langle \tilde{A}_i(t) \rangle_\Phi = \langle A_i(t) \rangle + i \int_0^t dt' \langle [V_I(t'), A_i(t)] \rangle + \dots, \quad (\text{A4})$$

where  $\langle \dots \rangle$  denotes an average with the initial density matrix  $\rho_0$ . For our choice of operators  $A_i$  the 0th order term in Eq. A4 vanishes. On introducing the response function

$$\chi_{ij}(t, t') = -i\Theta(t - t') \langle [A_i(t), A_j(t')] \rangle, \quad (\text{A5})$$

we finally find the Kubo formula. It states that in linear order the response of a system to the perturbation  $\Phi_j(t)$  is given by

$$\delta \langle \tilde{A}_i(t) \rangle = \int_0^t \chi_{ij}(t - t') \Phi_j(t') dt'. \quad (\text{A6})$$

In particular, if the perturbation is localized in time at  $t = 0$ , i.e.  $\Phi_j(t) = \Phi_j \delta(t)$ , then Eq. (A6) yields

$$\delta \langle \tilde{A}_i(t) \rangle = \sum_j \chi_{ij}(t) \Phi_j. \quad (\text{A7})$$

In this form it can be used to construct the corresponding quantum circuits as described in the main text.

## Appendix B: Non-linear response

In this Appendix we reconsider the measurement circuit on Fig. 9 at arbitrary strength of perturbation characterized by the angle  $\theta = \Phi_j^{\sigma'}$  and derive Eqs. (33) and (35).

To this end we introduce a wave function  $|\Psi_*\rangle$  to denote the initial state of a simulated Hubbard cluster at  $t = 0$ . It may or may not be equal to the VHA ground state  $|\Psi(\alpha_*, \beta_*)\rangle$  — the presented quantum algorithm for the Green's function measurement is independent of this. With the ancilla qubit taken into account, an initial state of the quantum circuit on Fig. 9 then reads  $|\Psi_0\rangle = |\Psi_*\rangle \otimes |1\rangle_d$ . When the perturbation Eq. (24) followed by the unitary evolution operator is applied to this state, it evolves into

$$|\Psi_t\rangle = (U_t \otimes e^{-\frac{i}{2}\lambda(ix_d y_d)}) e^{\frac{i}{2}\Phi_j^{\sigma'} y_{j\sigma'} x_d} |\Psi_0\rangle. \quad (\text{B1})$$

Here, the angle  $\lambda = \epsilon_d t$  and we have expressed the Hamiltonian of the  $d$ -fermion via Majorana operators,

$$H_d = \epsilon_d \left( d^\dagger d - \frac{1}{2} \right) \equiv \frac{i}{2} \epsilon_d x_d y_d. \quad (\text{B2})$$

With the state  $|\Psi_t\rangle$  at hand our aim now is to evaluate the response to the generalized force  $\Phi_j^{\sigma'}$  at time  $t$ ,

$$\langle A_i^\sigma(t) \rangle = \frac{i}{2} \langle \Psi_t | x_{i\sigma} x_d | \Psi_t \rangle, \quad (\text{B3})$$

beyond the linear regime discussed in the main text. Hence, we introduce Majorana operators of a cluster in the Heisenberg representation,

$$x_{i\sigma}(t) := U_i^\dagger x_{i\sigma} U_t \quad (\text{B4})$$

and use the anti-commutation relation of the ancilla Majorana  $x_d$  with its Hamiltonian, namely  $\{x_d, H_d\} = 0$ . The latter, in turn, yields a simple time evolution for  $x_d$ ,

$$x_d(t) := e^{\frac{i}{2}\lambda(ix_d y_d)} x_d e^{-\frac{i}{2}\lambda(ix_d y_d)} = x_d e^{\lambda(ix_d y_d)}, \quad (\text{B5})$$

where we reiterate that  $\lambda = \epsilon_d t$ . Definitions (B4) and (B5) enable one to rewrite the expectation value (B3) in a more transparent form,

$$\langle A_i^\sigma(t) \rangle = \langle \Psi_0 | e^{-\frac{1}{2}\Phi_j^{\sigma'} y_{j\sigma'} x_d} x_{i\sigma}(t) x_d(t) e^{\frac{1}{2}\Phi_j^{\sigma'} y_{j\sigma'} x_d} | \Psi_0 \rangle. \quad (\text{B6})$$

Further progress is feasible by observing that any bilinears of (unequal) Majoranas square to identity, e.g.  $(iy_{j\sigma'} x_d)^2 = (iy_d x_d)^2 = \mathbb{1}$ . As such, one may simplify the exponentials in (B6) as

$$e^{\frac{1}{2}\Phi_j^{\sigma'} y_{j\sigma'} x_d} = \cos \frac{1}{2}\Phi_j^{\sigma'} + y_{j\sigma'} x_d \sin \frac{1}{2}\Phi_j^{\sigma'}, \quad (\text{B7})$$

and use the analogous transformation to rearrange Eq. (B5). With the help of these relations the expectation value (B6) can be decomposed into eight terms. For each of these terms one performs an average in the ancilla's Hilbert space using the following relations

$$\begin{aligned} {}_d\langle 1|x_d|1\rangle_d &= {}_d\langle 1|y_d|1\rangle_d = 0, \\ {}_d\langle 1|ix_d y_d|1\rangle_d &= {}_d\langle 1|2d^\dagger d - 1|1\rangle_d = 1. \end{aligned} \quad (\text{B8})$$

As the result only four non-zero terms remain, which after straightforward algebra are simplified to

$$\begin{aligned} \langle A_i^\sigma(t) \rangle &= \frac{1}{2} \sin \Phi_j^{\sigma'} \sin \lambda \langle \Psi_* | \{x_{i\sigma}(t), y_{j\sigma'}\} | \Psi_* \rangle \\ &\quad - \frac{i}{2} \sin \Phi_j^{\sigma'} \cos \lambda \langle \Psi_* | [x_{i\sigma}(t), y_{j\sigma'}] | \Psi_* \rangle. \end{aligned} \quad (\text{B9})$$

To arrive at this expression one makes use of anti-commuting properties of Majoranas, i.e.  $\{x_{i\sigma}(t), x_d\} = \{x_{i\sigma}(t), y_d\} = 0$ . As one can see from Eq. (B9), by choosing the angle  $\lambda$  in the quantum circuit on Fig. 9 to be  $\pi/2$  or 0, the measurement outcome reproduces, respectively, either the retarded or Keldysh Green's function. Thereby we confirm one of our main results given by Eqs. (33) and (35).